Modeling the formation and migration of sand waves: The role of tidal forcing, sediment size and bed slope effects

Zhenlu Wang, Bingchen Liang, Guoxiang Wu, B.W. Borsje

PII: S0278-4343(19)30369-3

DOI: https://doi.org/10.1016/j.csr.2019.103986

Reference: CSR 103986

To appear in: *Continental Shelf Research*

Received Date: 23 October 2018

Revised Date: 29 September 2019

Accepted Date: 8 October 2019

Please cite this article as: Wang, Z., Liang, B., Wu, G., Borsje, B.W., Modeling the formation and migration of sand waves: The role of tidal forcing, sediment size and bed slope effects, *Continental Shelf Research*, https://doi.org/10.1016/j.csr.2019.103986.

Modeling the formation and migration of sand waves: The role of tidal forcing, sediment size and bed slope effects

Zhenlu Wang[1,2], Bingchen Liang[1,2,*], Guoxiang Wu[1,2], Borsje B. W.[3]

[1] College of Engineering, Ocean University of China, Qingdao, China

[2] Shandong Provincial Key Laboratory of Ocean Engineering, Ocean University of China, Qingdao, China

[3] Water Engineering and Management, University of Twente, Enschede, The Netherlands

Abstract：

Tidal sand waves are rhythmic bedforms existing widely in shallow shelf seas and are formed by the interaction of tidal currents and topography. Using a process-based numerical model, Delft3D, the wave lengths and migration rates of sand waves were simulated and verified with field measurements. The physical mechanism that controls the evolution of sand waves was mainly the balance between bedload transport, suspended load transport and the slope effect. It was found that the bedload transport multiplier, which reflects the bed slope effect, was a key parameter to reproduce the observed sand wave dynamics accurately. If the bedload transport multiplier is tuned with the actual grain size, it fits the observations on wavelength of sand wave much better. Both the migration rates and wavelengths were better predicted by the process-based numerical Delft3D model compared to a linear stability analysis sand wave model, since the former adopted sophisticated process formulations necessary for accurate field predictions. Next, sand wave formation and evolution under different environment settings, including tidal forcing and sediment sizes, were examined systematically. It was found that the preferred wavelength (L_{FGM}, fastest growing mode) of the sand wave increased with increasing tidal current magnitudes and decreasing sand diameters. Sand waves were only formed within a certain range and combination of tidal current magnitude and sand

diameters. Downstream- and upstream- migration of sand waves were predicted by considering residual currents or tidal constituent of higher harmonics.

Keywords: Sand waves; Delft3D; bed slope effect; migration rate; Morphodynamics; tidal forcing.

1. Introduction

The bed of shallow shelf seas inhabits regular bed forms of various sizes. According to their spatial scale, the bed forms can be categorized as sand ripples, sand waves or sand ridges (Németh et al., 2003). The wave lengths and heights of sand ripples are often too small (order of tens of centimeters) to influence the ocean engineering facilities (such as offshore underwater pipelines and cables) significantly. Tidal sand ridges typically have wavelengths of the order of 5~10 km and can be up to 30 m high, which is more than half of local water depth. The crests of sand ridges are usually rotated 10~30˚anticlockwise with respect to the principal tidal current direction in the northern hemisphere (Hulscher, 1996). Since sand ridges hardly move, they do not interfere with ocean engineering facilities. From an engineering perspective, more attentions are drawn to the sand waves with wave lengths of up to hundreds of meters, the heights of several meters, and the migration rates of up to several meters per year (McCave, 1971; Terwindt, 1971; Huntly et al., 1993; Borsje et al., 2014). The crests of the sand waves are almost perpendicular to the direction of the dominating currents (Besio et al., 2003). Sand wave migrations have a significant effect on many offshore activities, for example, the navigation, pipelines and cables, and sand mining (Németh et al., 2003; de Jong et al., 2016; Roetert et al., 2017). Understanding the characteristics of sand wave dynamics is therefore critical for smart and sustainable design in offshore operations (Damveld et al., 2016).

Theoretical model analysis and field observation were widely used in sand wave studies. The most prevalent model approach is the stability analysis, considering the sandy bottom and the hydrodynamic as a coupled

system to study whether regular features are associated with free instabilities of the system. Huthnance (1982) was the first to use this kind of model to predict the evolution of sand banks. However, no sand waves were found with the model which is probably because the vertical structure of the flow was neglected (Hulscher et al.,1993). The model was further improved and modified to include the vertical dimension by Hulscher et al. (1993,1996), enabling it to predict the typical characteristics of sand waves. Hulscher (1996) described the formation of sand waves as a free instability of sandy seabed subject to tidal motions. The formation mechanism of sand waves was explained by that the interactions of the oscillatory tidal flows with sinusoidal bed perturbations give rise to a tidally-averaged residual current, in the form of vertical recirculating cells directed from the trough to the crest of sand waves (Borsje et al., 2013). In the model proposed by Hulscher (1996) only bed load was considered, and a constant vertical eddy viscosity with a partial slip condition at the bed instead of no-slip condition was used. By introducing a height- and flow-dependent model for turbulent viscosity, Komarova et al. (2000) found long waves can be damped and a finite separation can be found which is agreement with the observed data. Besio et al. (2003) studied the effect of sediment characteristics on formation of sand waves. Next, many more physical processes were included in the model, such as graded sediment (Roos et al., 2007; van Oyen et al., 2009), suspended sediment transport (Blondeaux et al., 2005; Blondeaux et al., 2016), biology (Borsje et al., 2009a; 2009b; Damveld et al., 2019), and wind wave effects (Campmans et al., 2017). Moreover, models were developed to predict the migration of sand waves by including residual current (Németh et al., 2002) or different tidal components (Besio et al., 2004). In order to investigate the long-term behavior of sand waves, non-linear stability models were developed (Németh et al., 2007; van den Berg, 2007; van den Berg et al., 2012; Campmans et al., 2018).

Recently, process-based numerical models, such as Delft3D, ROMS (Zang et al., 2011), have been widely used

64 in the study of coastal morphodynamics. Tonnon et al. (2007) studied the morphodynamic behavior of an
65 artificial sand wave using Delft3D. Borsje et al. (2013, 2014) used Delft3D to study the formation mechanism
66 of sand waves, and investigated the effect of turbulence formulation and suspended sediment transport. The
67 role of suspended sediment transport and tidal asymmetry on the equilibrium sand wave height were further
68 examined by van Gerwen et al. (2018).
69 In summary, the models showed that the characteristics of sand waves (wavelength, growth rate, and migration
70 rate) depend on various environment factors, such as sediment grain sizes, tidal characteristics and the
71 associated residual currents. However, the sensitivity of sand wave dynamics to the environment factors is
72 hardly explored. The characteristics of sand waves and the environment parameters in two areas of North Sea
73 were summarized by Menninga (2012). With these field data, a Delft3D model was set up and verified. Next
74 the model was used to systemically investigate the role of variations in various environmental factors on sand
75 wave characteristics.
76 The aim of the paper is threefold: (1) to explain the main dynamic characteristics of sand waves in the
77 study-sites of IJmuiden area and Rotterdam area (Menninga, 2012) by applying a process-based numerical
78 model Delft3D, and compare it with a linear stability sand wave model of Blondeaux et al. (2016), (2) to
79 examine the sensitivity of sand wave characteristics to environment factors, (3) to investigate the migration
80 rates under different combinations of tidal components and related phase differences systematically and the
81 impact on wavelength of the sand wave. The remainder of the paper is organized as follows:
82 Section 2 introduces the model equations and model set-up. In section 3, the comparison between field data
83 and model results are given. Subsequently sensitivity of environment factors on characteristics of sand waves
84 are analyzed. Finally, section 4 and 5 contain the discussion and conclusions, respectively.

2. Methods and model description

2.1 Model formulation

The Delft3D modeling system consists of a hydrodynamic model based on the nonlinear shallow water equations, a suspended sediment and bedload transport model and a bed evolution model. Because most sand wave crests are oriented almost perpendicular to the tidal currents, the main physical process controlling the sand wave morphodynamics can be captured with the 2DV mode of Delft3D. Coriolis effects are assumed to have a negligible effect on the evolution of sand waves (Hulscher, 1996) and therefore not taken into account in the sand wave model. The basic hydrodynamics equations are given in Appendix A.

Sediment can be transported as bedload and suspended load. Sediment transport and morphological evolution equations are given in Appendix B. A detailed model formulations and solutions can be referred to Lesser et al. (2004) and Delft3D Flow manual.

2.2 Model set-up

The length of the model domain is about 50 km. 6 km of sand waves are designed to lay in the center of the model domain. The horizontal grid size in the sand wave area is 10 m and increases gradually up to 1500 m at the lateral boundaries (Figure 1(a)). In the vertical dimension, 20 σ-layers is set with high resolution near the bed and decreasing towards to the water surface (Figure 1(b)). The initial amplitude of the sand waves is 0.5 m, which is small compared with the water depth. The sand wave field is multiplied by a tapering function to create a transition region from the sand wave domain to flat-bed. Riemann boundary conditions are imposed at lateral boundaries so that the tidal waves can travel out of the model domain without reflecting back. We used S2 tide instead of M2 for the convenient with the FFT analysis, because the tidal period of this constituent is exactly 12 hours. Also, we considered M0 tide (residual current) and the S4 tide (instead of M4) as the input

parameters. The Chézy coefficient is set to a constant value of 65 $m^{1/2}/s$ (Borsje et al., 2013). The time step is 12 s, and the model runs for two tidal circles. In the first tidal circle, only hydrodynamics is calculated to achieve a steady state (spin-up time), then in the second tidal circle bed updating is activated. The bed evolution can be described as $z_b = A(t)\exp(2\pi i x / L) + c.c.$ (here L is the sand wave length). Assuming exponential growth (Besio et al., 2008; Borsje et al., 2013), the growth rate γ_R and migration rate γ_I is calculated by:

$$\gamma_R = \frac{1}{T}\mathrm{Re}\left(\log\left(A1/A0\right)\right) \quad (1)$$

$$\gamma_I = \frac{-1}{kT}\mathrm{Im}\left(\log\left(A1/A0\right)\right) \quad (2)$$

The model parameters used was presented in Table 1.

Table 1. Overview of values of model parameters.

Description	*symbol*	*value*	*unit*
gravity acceleration	g	9.81	m/s^2
Chézy roughness	C_D	65	$m^{1/2}s^{-1}$
water density	ρ_w	1025	kg/m^3
sediment density	ρ_s	2650	kg/m^3
Kármán's constant	κ	0.41	-
bed porosity	p_{or}	0.4	-
initial sand wave amplitude	A_0	0.5	m

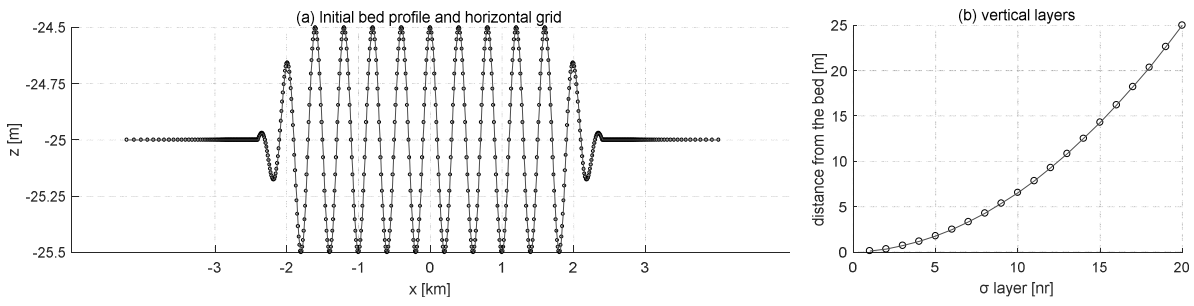

Figure 1. the grid set-up with (a) initial bed profile for wavelength of 400 m sand wave and the horizontal grid using

the fine grid in the center 6 km where the sand waves calculated and a coarser grid towards the boundaries and (b) the distribution of vertical σ-layers over the water depth. Note that the wavelength of the initial bed profiles varies in a range to determine the fastest growing mode and the water depth changed for the different model simulations.

2.3 Environment parameters and characteristics of observed sand waves

The model presented above was used to investigate the effects of suspended sediment transport (Borsje et al., 2014) and different turbulence formulations (Borsje et al., 2013) on the formation of sand waves. The model showed fairly good agreement with field data qualitatively. As Figure 2 shows, data sets of two areas in the North Sea was collected and analyzed by Menninga (2012). IJmuiden area comprises 170 km^2, with latitudinal coordinates (in UTM-WGS84) ranging from 5810100 to 5820200 and longitudinal coordinates from 546500 to 604200, and Rotterdam area comprises 310 km^2, with latitudinal coordinates ranging from 5742600 to 5766300 and longitudinal coordinates ranging from 476900 to 564300.

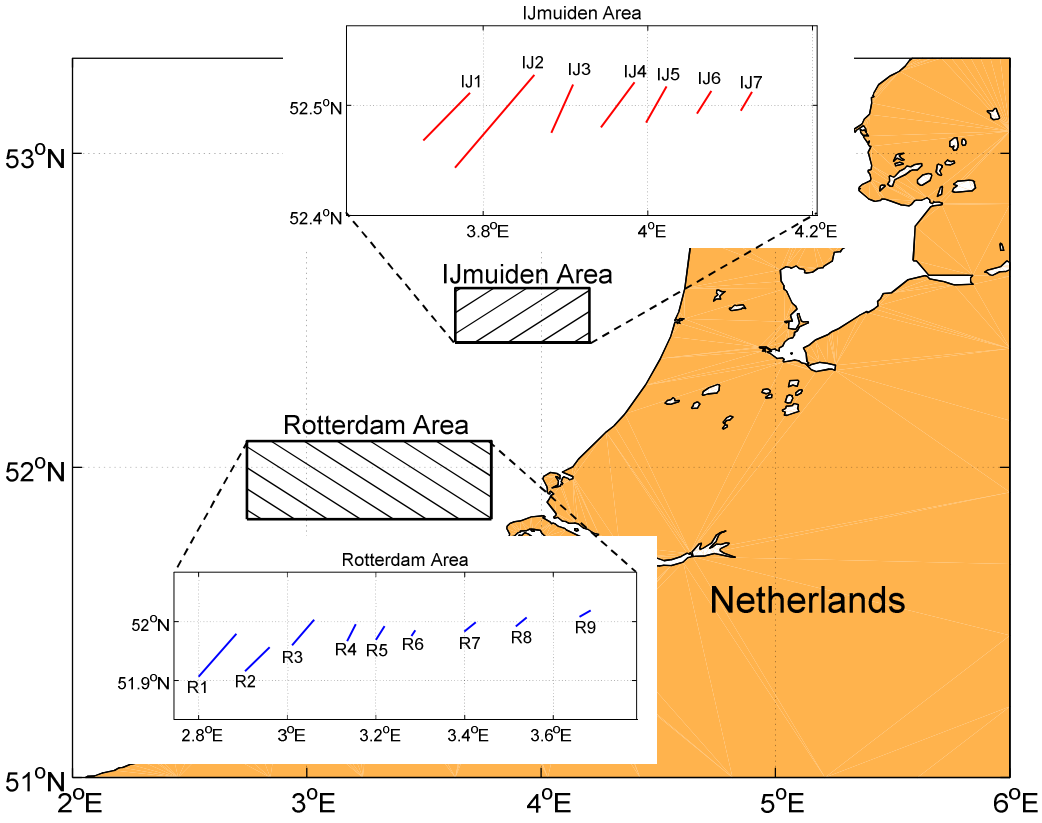

Figure 2. Study areas: IJmuiden area and Rotterdam area (adapted from Menninga (2012)).

Table 2 shows the environmental parameters at two sites in the North Sea collected by Menninga (2012), namely, IJmuiden area (denoted by IJ-, including 7 sites), and Rotterdam area (denoted by R-, including 9 sites), respectively. The two sites have quite different environmental parameters, and the water depth in Rotterdam area is between 26.6~36 m, which is larger than that in IJmuiden (23.6~27 m). The tidal-velocity amplitude in IJmuiden area is between 0.63 m/s and 0.66 m/s which is smaller than that in Rotterdam area (0.69~0.79 m/s). The mean sediment diameter in Rotterdam area is about 0.358 mm, which is also larger than that in IJmuiden (0.284 mm). The characteristics of sand waves are different in two areas. The main difference in characteristics of sand waves is that the wave length and the migration rate in IJmuiden area are both larger than those in Rotterdam area. Refer to Menninga (2012) and Blondeaux et al. (2016) for more details on

141 environmental parameters and characteristics of sand waves.

142 Table 2. Environmental parameters and Characteristics of sand waves of two sites (Menninga, 2012)

Site	H(m)	d_{50} (mm)	U_{M2} (m/s)	ecc_{M2}	U_{M4} (m/s)	ecc_{M4}	$\Phi_{M2\text{-}M4}$ (degrees)	U_{M0} (m/s)	L_{sw} (m)	H_{sw} (m)	c_{crest} (m/year)	c_{trough} (m/year)	c_{mean} (m/year)
IJ1	27.0	0.309	0.66	0.018	0.047	0.51	339	0.019	380	3.4	2.4	0.2	1.30
IJ2	26.5	0.308	0.66	0.009	0.047	0.54	342	0.018	395	3.3	2.3	-0.1	1.10
IJ3	26.0	0.288	0.65	0.001	0.046	0.58	346	0.019	450	3.4	2.6	0.2	1.40
IJ4	24.5	0.278	0.64	0.006	0.046	0.62	352	0.018	428	2.6	2.8	0.4	1.60
IJ5	24.3	0.268	0.64	0.011	0.045	0.64	355	0.017	395	2.3	3.3	0.4	1.85
IJ6	23.8	0.271	0.63	0.012	0.043	0.67	354	0.022	310	1.5	3.1	1.2	2.15
IJ7	23.6	0.266	0.63	0.005	0.041	0.76	0.84	0.029	615	2.8	2.7	0.2	1.45
R1	36.0	0.445	0.79	0.11	0.060	0.07	115	0.019	315	4.0	-0.1	0.0	-0.05
R2	35.4	0.421	0.73	0.11	0.053	0.09	130	0.04	200	3.2	0.1	0.0	0.05
R3	33.3	0.398	0.71	0.10	0.054	0.11	124	0.044	270	4.1	0.4	0.3	0.35
R4	32.6	0.372	0.73	0.11	0.057	0.16	122	0.041	220	3.5	0.7	0.5	0.60
R5	31.8	0.317	0.72	0.11	0.056	0.19	121	0.039	205	3.1	1.0	0.9	0.95
R6	32.0	0.332	0.72	0.12	0.057	0.21	120	0.039	225	3.3	0.7	0.6	0.65
R7	29.0	0.306	0.71	0.12	0.057	0.25	116	0.039	245	3.6	1.0	1.5	1.25
R8	28.4	0.336	0.69	0.12	0.058	0.27	110	0.034	250	3.3	1.0	0.9	0.95
R9	26.6	0.301	0.67	0.11	0.059	0.27	102	0.034	315	2.1	2.1	2.1	2.10

143 where H is water depth, d_{50} is the median sediment diameter, U_{M2} is the amplitude of M2 tidal current,
144 ecc_{M2} and ecc_{M4} are M2 ellipticity and M4 ellipticity respectively, U_{M4} is the amplitude of M4 tidal current,
145 ϕ_{M2-M4} is the phase between M2 and M4 tide, U_{M0} denotes the residual current, L_{sw} and H_{sw} are the
146 wavelength and height of sand waves respectively, c_{crest}, c_{trough}, c_{mean} are the crest/trough/mean migration rate
147 of sand waves.

148 Predictions using a stability analysis matched the field data qualitatively in terms of various characteristics of
149 the sand waves (Blondeaux, 2016). In their model the wind waves and different tide constituents were taken
150 into account, a time-independent eddy viscosity function was used to close the hydrodynamic problem, and
151 suspended sediment transport was included in addition to bedload transport. In their stability analysis model,
152 default values were used for all parameters, although the values of some key parameters (such as sediment

153 sizes) fall into a large range. Considering that modeled sand wave dynamics may be very sensitive to these
154 environment parameters, in this study we use the Delft3D model to analyze the characteristics of the sand
155 waves systematically with different settings of environmental parameters and sediment characteristics.

156 **3. Results**

157 3.1 Model validation: Comparison with field data

158 The model was established using the environmental parameters of case IJ3 and case R3 in the Table 2,
159 respectively. Bed evolution was calculated with different sand wave numbers as the initial bed level. For the
160 IJ3 case, the slope factor α_{bs} was set to 1.4. With Fast Fourier Transform (FFT) analysis, the relationship
161 between sand wave growth rates and sand wave numbers was obtained, as summarized in Figure 3 (a). The red
162 dot represents the fastest growing mode, which corresponds the preferred wavelength of the sand wave under
163 the specified environmental parameters. From Figure 3 (a), the L_{FGM} reads 450 m which matches perfectly
164 with the observed data. The migration rates versus sand wave numbers are shown in Figure 3 (b). The
165 migration rate corresponding to the fastest growing mode (red dot) is 1.1 m/year, which is close to the
166 observed migration rate of 1.4 m/year. The same method was used on R3 case, with the same slope factor of
167 1.4, the L_{FGM} reads 400 m which is much larger than the observed data (270 m). After calibrating the model
168 with the slope factor of 1.0, it turns out a better prediction of L_{FGM} (290 m). The migration rate is 1.49 m/year
169 with slope factor of 1.0, which is almost the same (1.51 m/year) as that with a slope parameter of 1.4.

170 The verified model was used on other sites of the two areas to calculate the preferred wavelength and
171 migration rate of the sand wave. As the first 7 sites located the same area, i.e. IJmuiden, we used the same
172 slope factor of 1.4. For the rest 9 sites located in the Rotterdam area, the slope factor of 1.0 was used.
173 Blondeaux et al. (2016) used stability analysis model to study the characteristics of sand waves and the results

174 can be found in Table 3. The results of numerical simulation we used are also listed in Table 3.

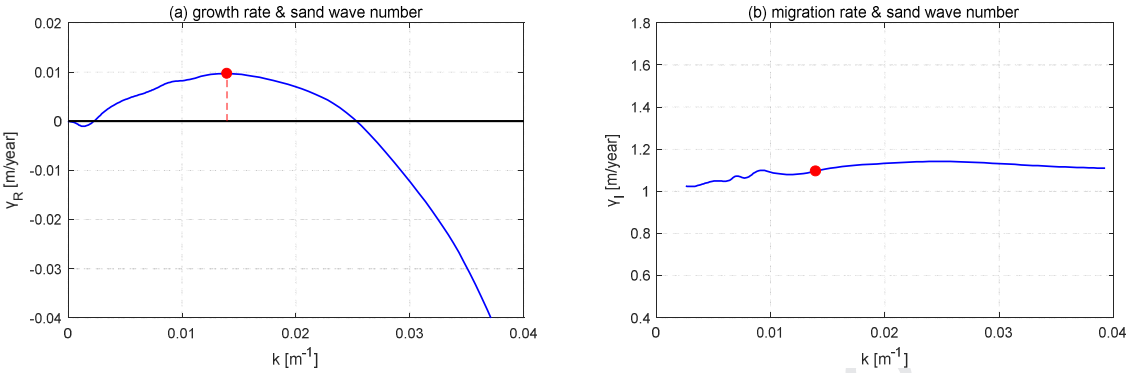

175

176 Figure 3. Growth rates (a) and migration rates (b) under different sand wave numbers. The curves are corresponding

177 to the case of J3 and the red dot indicates the fastest growing mode.

178 Table 3 Sand wave characteristics predicted in Blondeaux et al. (2016) and in this study

	results in Blondeaux et al. (2016)		results in this study	
Site	L_{sw_S} (m)	c_S (m/year)	L_{sw_N} (m)	c_N(m/year)
IJ1	386	3.77	387	2.73
IJ2	387	3.63	400	2.72
IJ3	430	3.44	450	1.10
IJ4	453	3.18	374	2.77
IJ5	492	2.85	413	2.70
IJ6	467	3.45	374	2.91
IJ7	494	4.39	350	3.34
R1	233	-0.35	270	-0.09
R2	332	3.91	276	1.17
R3	337	4.32	290	1.63
R4	315	4.29	306	1.49
R5	434	4.00	283	1.35
R6	394	3.76	298	1.39
R7	434	4.08	270	1.59
R8	337	2.67	283	1.39
R9	418	2.63	270	1.68

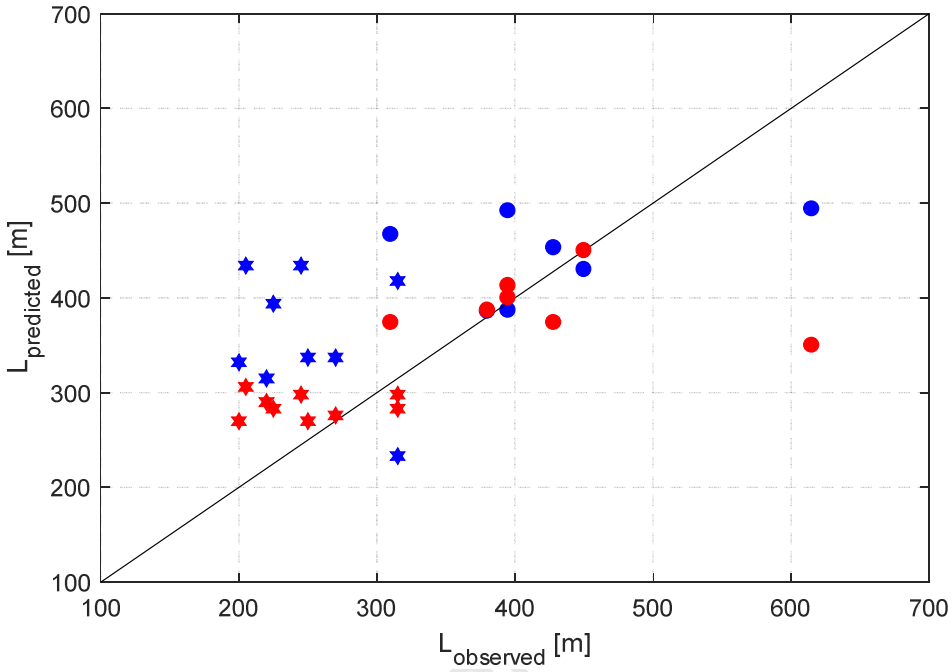

Figure 4. Comparison of predictions on wavelengths of sand waves by the stability model (blue marks, dots for IJmuiden site and hexagrams for Rotterdam site, Blondeaux et al. 2016), Delft3D (red marks, dots for IJmuiden site with α_{bs} = 1.4, hexagrams for Rotterdam site with α_{bs} = 1.0).

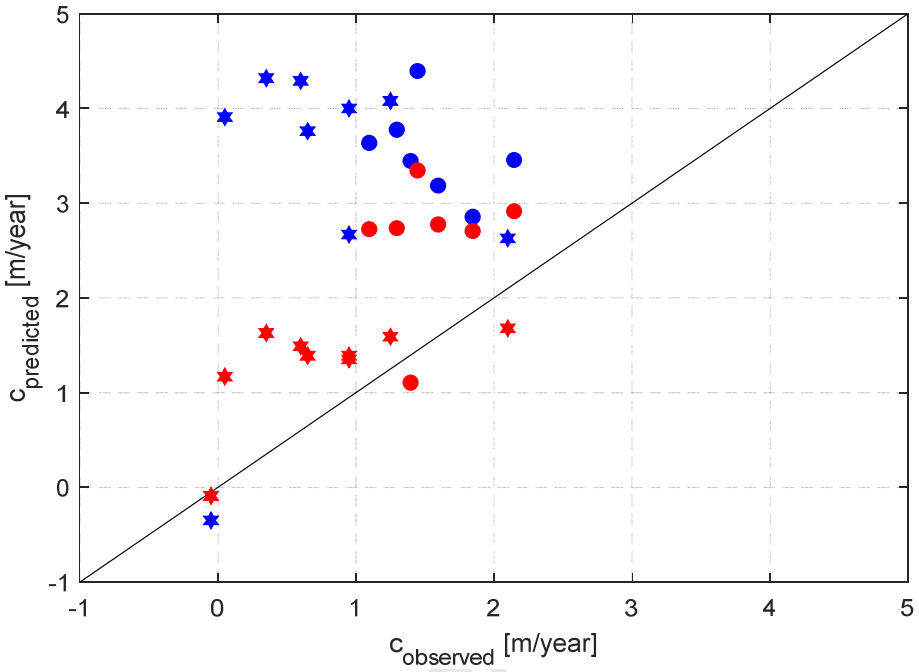

Figure 5. Comparison of predictions of sand wave migration rates by the stability model (blue marks, dots for IJmuiden site and hexagrams for Rotterdam site, Blondeaux et al. 2016), Delft3D (red marks, dots for IJmuiden site with α_{bs} = 1.4, hexagrams for Rotterdam site with α_{bs} = 1.0).

Figure 4 shows the predicted wavelengths of sand waves of stability model and Delft3D versus observed field values. All the predicted values seemed well agreement with the observed values qualitatively. Three indexes, namely, the Bias, the Root-mean-square-errors (RMSE), and the Correlation relationship, were used to make quantitate comparisons between the two models.

$$Bias = \frac{1}{N_d}\sum_{i=1}^{N_d}\left(S_i - M_i\right) \tag{3}$$

$$RMSE = \sqrt{\frac{1}{N_d}\sum_{i=1}^{N_d}\left(S_i - M_i\right)^2} \tag{4}$$

$$r = \frac{\sum_{i=1}^{N_d}\left[\left(S_i - \bar{S}\right)\left(M_i - \bar{M}\right)\right]}{\sqrt{\sum_{i=1}^{N_d}\left(S_i - \bar{S}\right)^2 \sum_{i=1}^{N_d}\left(M_i - \bar{M}\right)^2}} \quad (5)$$

where N_d is the total number of the values of observations and predictions, S_i is the predicted value and M_i is the observed value. Bias is also referred as the mean error. A smaller Bias value indicates a better agreement between observed and predicted values. The r denotes the correlation coefficients.

Table 4. statistical indicator values for characteristics of sand waves

Statistical indicators	Test[a]	Values for wave length of sand waves	Values for migration of sand waves
RMSE	T1	117.9	2.56
	T2	81.2	0.99
Bias	T1	70.3	2.27
	T2	6.5	0.76
R	T1	0.51	0.16
	T2	0.69	0.68

[a] Two tests are performed, and test T1 represents for the stability results of Blondeaux et al. (2016). T2 represent for numerical results in this paper, α_{bs} =1.4 for IJmuiden area and 1.0 for Rotterdam area.

Table 4 shows the statistical indicator values for characteristics of sand waves. For the wave length of the stability model, RMSE is 117.9, Bias is 70.3 while the correlation coefficient is 0.51. For the numerical model, the indicators are 81.2, 6.5 and 0.69 respectively when the slope factor α_{bs} is 1.4 for IJmuiden area and 1.0 for Rotterdam area. The prediction of wave lengths of sand waves was much better using the numerical model. The same method was used to estimate the difference between predicted values and observed values of migration rate (Figure 5). For the stability model, the values of three indicators are 2.56, 2.27 and 0.16 which means predicted values are not in agreement well with observed values. Then for numerical model the three indicators are 0.99, 0.76 and 0.68 respectively. These values are much better than that predicted by stability

models. With different slope factors in two areas, a better prediction on wavelengths and migration rates of sand waves can be obtained.

The bed slope effect can change the transport rate once the sediment is in motion (van Rjin, 1993). This effect can be formulated by Equation. 28 in Appendix B. In general, the repose angle of coarser sand is larger than finer sand which will induce the slope coefficient α_s smaller. From Equation. 28 of Appendix B we can use a smaller slope factor α_{bs} to tune the slope coefficient α_s smaller. As can be found in Table 2, the sediment diameter in the Rotterdam site is larger than that in the IJmuiden site, so it is reasonable to use a smaller slope coefficient for the Rotterdam area.

3.2 The effects of bed slope

The effects of different slope factors on sand wave growth and L_{FGM} were examined. A series of idealized model settings were designed, in which only an S2 tide was considered. Other parameters were kept fixed as follows: H = 25 m, U_{S2} = 0.65 m/s, d_{50} = 0.35 mm. These parameters resemble a typical North Sea situation for sand wave occurrence (Borsje, et al., 2009a). We varied the slope factor α_{bs} in the range of 0 ~ 3.5 with an interval of 0.5.

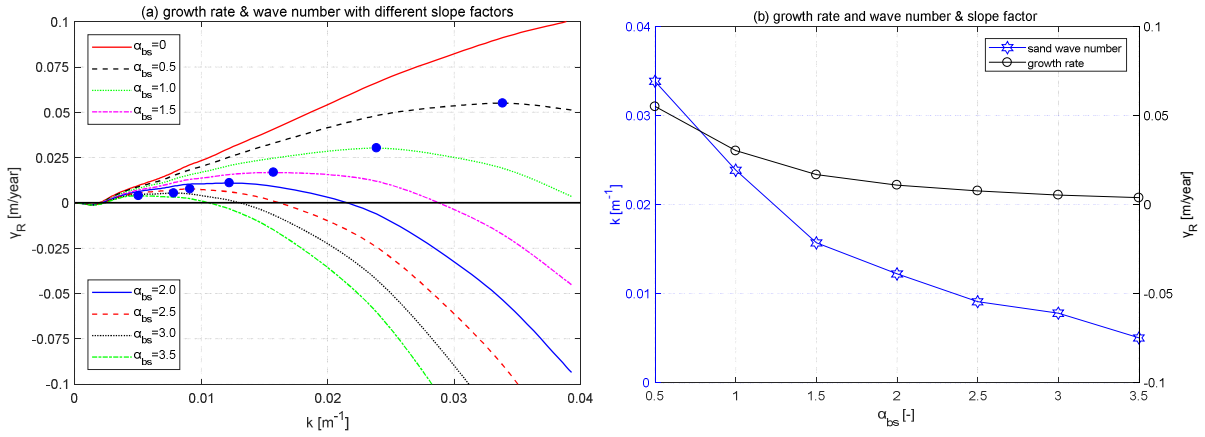

Figure 6. (a) The growth rates versus sand wave numbers with different slope factors, the blue dots indicating the

fastest growing mode. (b) The growth rates and sand wave numbers versus slope factors under the fastest growing mode conditions.

As Figure 6(a) shows, without considering slope effect (i.e. α_{bs} = 0), the sand waves will always be growing in the range of the specified sand wave numbers of 0~ 0.04. For large wave numbers, the tide-averaged vertical circulation flow is strongest (Borsje et al., 2013) leading to the largest growth of the sand waves. However, when the slope factor α_{bs} is larger than 1.0, the curves between the growth rate and sand wave number start to display the parabolic shape as a result of slope-induced transport. A critical point exists at the peak of the parabolic (blue dots in Figure 6(a)) which represents the fastest sand wave growth rates. The bed slope effect acts as a decaying mechanism which makes the upslope sand transport more difficult than downslope transport. The decaying mechanism will be enhanced under a larger slope factor, resulting in a slower growth rate. Besides, the range of possible wavelengths of sand waves will be narrower under a larger slope factor.

Figure 6(b) shows the relationship of growth rates and the preferred wave numbers of sand waves versus slope factors. It is clear that the wave length decreased rapidly while the growth rate of sand waves only decreases slightly with the increase of the slope factor. When the slope factor is large enough, the sand waves hardly grow.

3.3 The effects of tidal currents and sediment sizes

The effects of different tidal currents and sediment sizes on sand wave growth and L_{FGM} were examined. Two series of numerical experiments were carried out. For the first series, some parameters were kept fixed as follows: H = 25 m, d_{50} = 0.35 mm, α_{bs} = 1.5. We varied the amplitude of tidal currents in the range of 0.4~1.2 m/s with interval of 0.05 m/s. For the second series, the parameters were kept fixed as follows: H = 25 m, U_{S2} = 0.65 m/s, α_{bs} = 1.5. We varied the sediment sizes in the range of 0.15~0.55 mm with an interval of

0.05 mm.

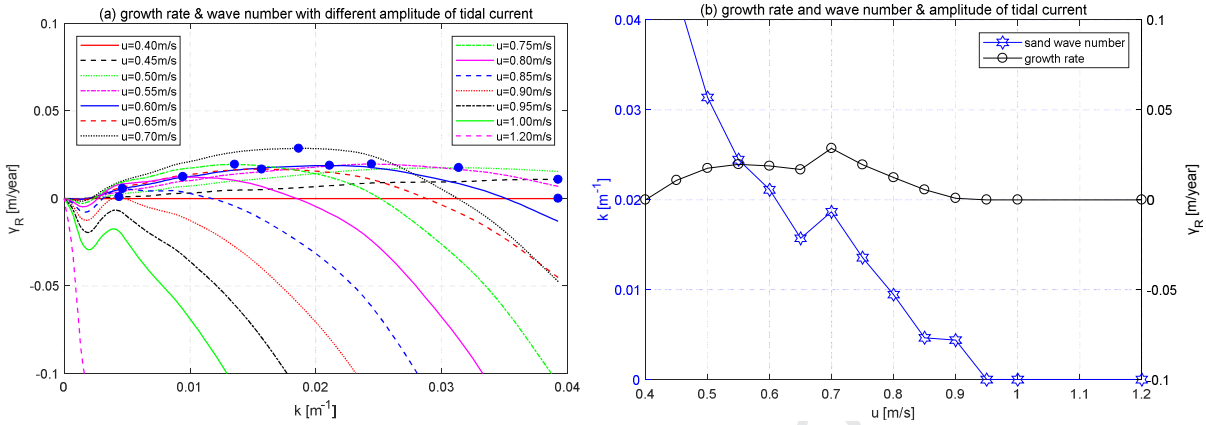

Figure 7. (a) the growth rate versus sand wave number with different amplitude of tidal currents and the blue dots indicate the fastest growing mode. (b) the growth rate and sand wave number versus amplitude of tidal current under the fastest growing mode conditions.

The red solid line in Figure 7(a) shows that the sediment stayed still when the tidal current strength was less than 0.4 m/s. For increasing tidal amplitudes of the tidal current, sediment will start to move as soon as the bed shear stress became larger than the critical bed shear stress. When the amplitude of tidal current was larger than 0.45 m/s, the sand waves keep growing in the range of specified wave numbers. The fastest growing mode (blue dots) appeared in a specific range of the tidal currents. On the other side, if the velocity was too large (larger than 0.9 m/s in this study), the growth rate of sand waves stays negative, indicating that no sand waves were formed. This test also proved that sand waves can only be formed within certain range of tidal current magnitudes in accordance with previous studies (Borsje et al., 2014). Generally, the range of the wavelength of the sand wave which may be appeared will become narrow with the increase of the tidal current strength until the sand waves disappear. Figure 7(b) shows the sand wave number and the growth rate of fastest growing mode under different tidal current magnitudes. The growth rates first increased, and then decreased, with

increasing tidal currents. For this parameter setting, the maximum value occurred at the tidal velocity of 0.7 m/s. When the velocity was smaller, less sediment was moved thus the growth rates of sand waves were small as well. When the velocity was larger, most sediment moves as suspended load, which may decay the growth of the sand waves (Borsje et al., 2014). The wavelength of the sand wave increased rapidly in general with increasing tidal currents. Note there appears a slight discontinuous behavior when the amplitude of tidal current is 0.7 m/s. This is due to a combination of bedload transport and suspended sediment transport. With increasing tidal currents, the growth rate of sand waves due to bedload increases while the growth rate due to suspended sediment decreases. There is a small difference in the rate of increase and decrease which induced the discontinuous behavior. As shown in Figure 7, the sand wave most likely occurred in the range of 0.45~0.9 m/s for this parameter setting.

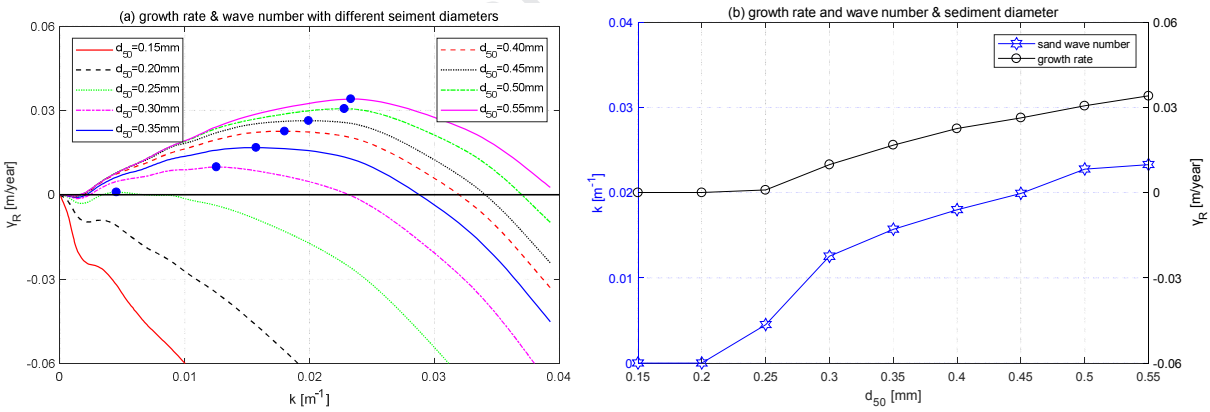

Figure 8. (a) the growth rates versus wave numbers with different sediment diameters and the blue dots indicate the fastest growing mode. (b) the growth rates and the wave numbers of sand waves versus sediment diameters under the fastest growing mode conditions.

It is found from Figure 8(a) that when the sediment diameter was smaller than 0.2 mm, no sand waves were formed and all sand waves decayed, resulting in a flat bed. It is because that suspended load dominates when

277 the sediment diameter is small, preventing the formation of sand waves. The growth rates become positive and
278 the sand waves appear when the sediment diameter is larger than 0.25 mm. As the sediment diameter continued
279 to increase, bedload transport began to dominate, which promotes sand waves growth. As shown in Figure 8(a),
280 the range of possible wavelengths of sand waves was generally wider for larger sediment diameters. Figure 8(b)
281 shows the sand wave numbers and growth rates of the fastest growing mode versus sediment diameters. The
282 growth rate of the sand wave increased and the wavelength decreased with the increase of the sediment
283 diameter. To conclude, our simulations showed that finer sediment tend to produce longer wave lengths, while
284 coarser sediment tend to produce shorter wave lengths.

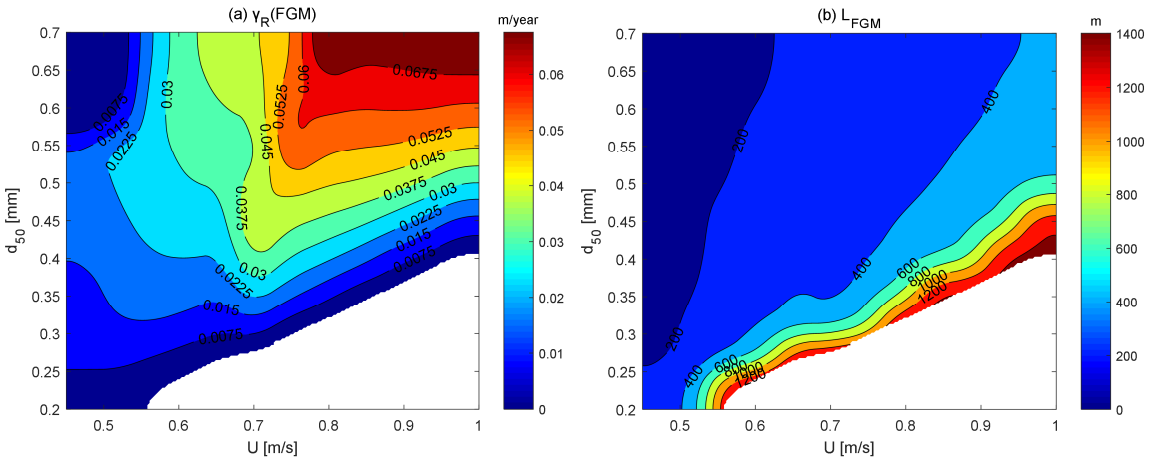

285

286 Figure 9. (a) the relationship between growth rate of fastest growing mode and sediment diameter and tidal current.
287 (b) the relationship between preferred sand wavelength and sediment diameter and tidal current.

288 Simulations with different combinations of sediment diameters and tidal currents were further conducted. The
289 water depth was 25 m, and the slope factor was set to 1.5. Figure 9 shows that at the upper left and lower right
290 the sand waves are absent. When the velocity is weak and the sediment is coarse (the upper left), the sediment
291 hardly can move by the tidal current, so the bed form will maintain stable. When the velocity is too strong and
292 the sediment is fine (the lower right), the dominated sediment transport is suspended load transport which

damps the growth of the sand waves, the bed form also stays stable. The parameters of the most likely appearance of the sand waves are coarser sediment and relative lager tidal current which can be found at the upper right of the Figure 9(a). Figure 9(b) shows the wavelength of fastest growing mode of sand waves mainly in the range of 200 m to 600 m. The longer wavelength of sand waves appears on the condition of the high velocity and fine sediment where the suspended sediment transport dominate the bed form evolution. Previous research and observed field data indicate that the wavelength is up to hundreds of meters which support the results here we found.

3.4 Sand wave migration: the role of tidal asymmetry

Sand waves can be formed and grow under a symmetry tide (such as the S2 used in above simulations). However, sand wave migrations may occur in case of the distortion and loss of tidal symmetry. Here we analyzed the relationship between sand wave migrations and tidal asymmetry. Two series of numerical experiments were conducted. In the first series only an S2 tide was considered, the parameters were kept fixed as follows: H = 25 m, U_{S2} = 0.65 m/s, d_{50} = 0.35 mm, α_{bs} = 1.5. We varied the residual currents in the range of 0~0.3 m/s with an interval of 0.05 m/s. In the second series, the parameters were kept fixed as follows: H = 25 m, U_{S2} = 0.65 m/s, d_{50} = 0.35 mm, U_{S4} = 0.05 m/s, α_{bs} = 1.5, and the residual current were set to 0 m/s. We varied the phases of S4 tide in the range of 0~360° with an interval of 30°.

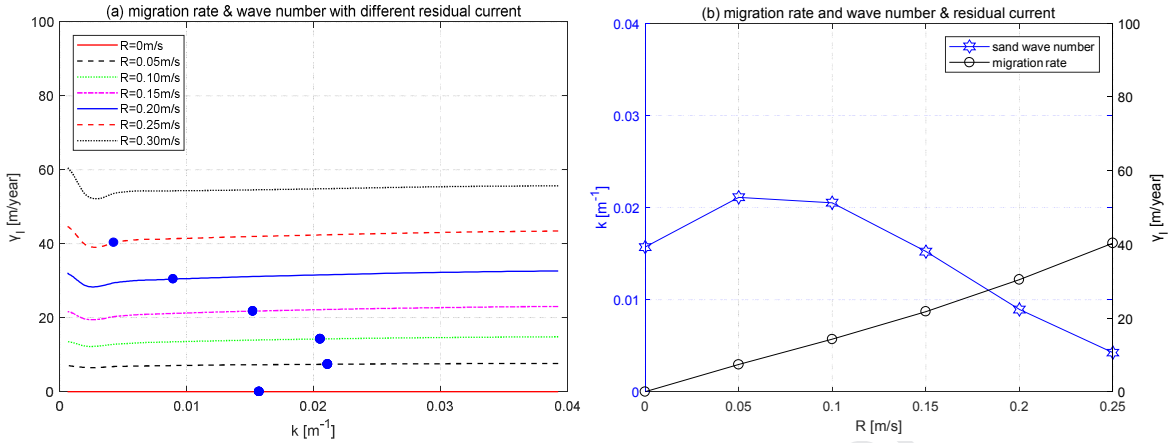

309

310 Figure 10. (a) the migration rate versus wave number with different residual current and the blue dots indicate the

311 fastest growing mode. (b) the migration rate and the wave number of sand waves versus residual current under the

312 fastest growing mode conditions.

313 The red line in Figure 10(a) shows that no migration occurs under a single S2 tide. When the residual currents

314 are added, sand waves start to migrate in the direction of the residual currents. The symbols in Figure 10(b)

315 corresponding to the fastest growing mode which is the most preferred bed forms that may appear. It is found

316 that migration direction always followed the direction of residual currents and the migration rates increased

317 with increasing residual currents. However, when the residual current was too strong, the fastest growing mode

318 disappeared, as shown by the black dash line in Figure 10(a). The wavelength of the sand wave first increased

319 and then decreased with the increase of the residual currents.

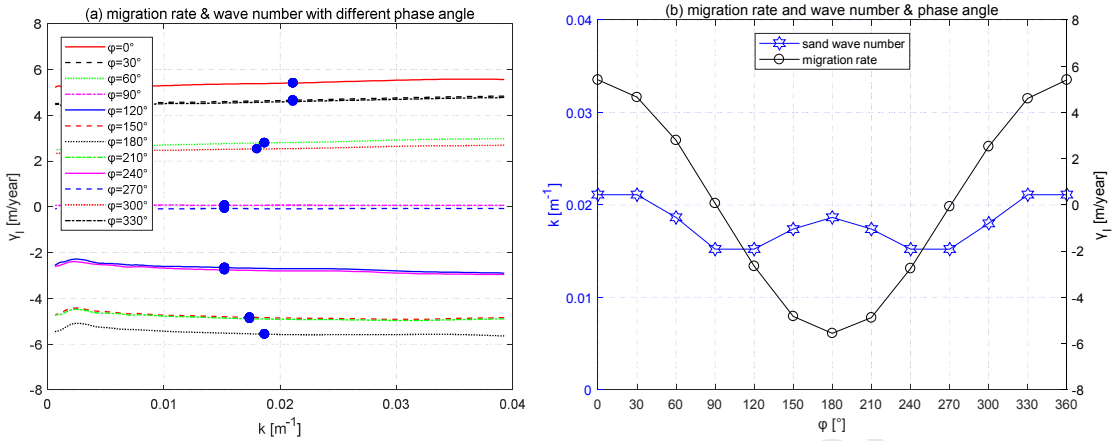

Figure 11. (a) the migration rate versus wave number with different phases between S2 and S4 and the blue dots indicate the fastest growing mode. (b) the migration rate and the wave number of sand waves versus phases under the fastest growing mode conditions.

Previous studies suggested that the migration direction of the sand waves may be opposite to the residual current (Besio, 2004). Figure 11 shows the migration rate of sand waves with different phases between the tide component S2 and S4. The curve of sand wave number and migration rate corresponding to fastest growing mode is symmetrical on both side taking 180° as the centerline. When the phase is 90° or 270°, the sand wave cannot migrate. While the phase is falling in the scope of 90°~270°, the migration direction will be negative. Although the current induced by S2 and S4 tide constituents will vanish during the time averaged, the nonlinear relationship between fluid velocity and the sediment transport will induce the sand waves move towards a specific direction. As a result, the migration direction of the sand waves will depend on the relative intendance of phase of different tidal components and residual current. If the residual current is small and the higher harmonic tidal component is large or the phase between tidal components is appropriate, then migration direction of sand waves may be opposite to the residual current. The L_{FGM} varied according to the phases between the tidal components. The L_{FGM} decreased with the increasing of the migration rate no matter the sand

wave migrates forward or backward. When the phase is 90°, the wave length is the longest and the sand wave cannot migrate.

4. Discussion

In this paper, we studied the effect of some environment parameters on formation and migration of sand waves. The model was calibrated with slope factor for two specific sites, the wavelength of the sand wave is reproduced good compared to observed data. The migration rate is considerably better predicted with the numerical model compared to the Blondeaux et al. (2016) model. In Blondeaux et al. (2016), the eddy viscosity was assumed to be time-independent following Besio et al. (2006). The eddy viscosity we used in the Delft3D model was derived from a more accurate turbulence formulation ($k-\varepsilon$), and it may gave a better prediction on the wavelengths and the migration rates of sand waves.

In general, the migration rate of sand waves in IJmuiden is larger than that in Rotterdam area for both the field data and model results. As discussed above, the migration of sand waves is mainly caused by residual currents and tidal asymmetries which typically result from different tidal components and phases. In the IJmuiden area, the phase between M2 and M4 is 339°~0.84°, under which the migration of sand waves is positive according to Figure 9(b). The migration direction controlled by the residual current is also positive, so the sand waves move at a fast rate in the direction of the residual current. On the other side, in the Rotterdam area, the phase of M2 and M4 is 102°~130°, resulting in a negative migration of sand waves based on Figure 11.

The negative effect exerted by tidal phases counteracts the positive effect induced by residual currents, thus the migration rates are smaller in the Rotterdam area compared with that in the IJmuiden area. Take the parameters of R1 site for example in the Table 2, the negative effect induced by the tidal components' interaction overwhelms the positive effect caused by residual currents, making the sand waves migrate in the opposite

direction of the residual current (0.019 m/s). Then focus on R2 site, the residual current (0.04 m/s) is much larger than that in R1 site. The positive effect overwhelms the negative effect which may makes the sand waves migrate in the direction of the residual current. The difference of quantitative results between the migration rate of observed data and model data in IJmuiden area may be caused by the approach of evaluation of the migration. Table 2 also shows that in Rotterdam area crest and trough migration is almost the same while in the IJmuiden area there is quite difference in crest and trough migration. The mean migration rate of the observed data was obtained by the average of the crest and trough migration which may be underestimated compared with the model result which was evaluated by FFT analysis.

According to van Santen et al. (2011), the wavelength of sand waves decreased with increasing grain size which concurs with the results of our model. However, in their study, the larger tidal current amplitudes will induce the decrease of tidal sand wavelength which is opposed to ours. They only used the bedload transport to evaluate the sediment transport while the suspended sediment transport was also included in our model. The suspended transport may induce the longer wavelength of sand waves as discussed by Borsje et al. (2014). So, when the tidal current amplitude was large, suspended transport would be the dominant transport which may cause the longer wavelength.

The role of wind waves was not included in our model which may influence the prediction of characteristics of sand waves (Campmans et al., 2017). The interaction between surface wave and the tidal current may results the change of the flow fields. The nonlinear of wave action in shallow water should not be neglected on the sediment transport. So, a next step is to study the role of wind waves in the formation and evolution of sand waves with the process-based model Delft3D.

5. Conclusions

The sand wave dynamics were investigated with a process-based numerical model, Delft3D. Two sites in the North Sea were used for model validations. The sensitivities of modeled sand save growth and migration to environmental settings and model parameters, namely, sediment sizes, tidal currents and tidal asymmetries, and bed slope effects, were examined systematically.

The conclusions can be summarized as follows:

1. The numerical model is effective to research the characteristics of the sand waves, including wave length and migration rate of sand waves. The bed slope factor is critical to predict the wavelength and migration rate of sand waves and need to be calibrated and is related to the local sediment grain size. In general, when the grain size is finer, a higher slope factor can be adopted to perform a better result in predicting the characteristics of sand waves.
2. Sensitive analysis of environment parameters shows that the preferred wavelength increased and the corresponding growth rate decreased with the increase of bed slope factors. In general, the sand waves were absent when the tidal current was too large and the sediment was too fine. The preferred wavelength of sand waves decreased with the increase of the sediment diameter and the decrease of tidal current. For coarser sediment, the growth rate of sand waves will increase first and then decrease with the increase of the tidal current. For finer sediment the growth rate will always decrease with the increase of the tidal current.
3. The interaction between the residual current and the tidal components can explain the migration of sand waves. Considering the phases between different tidal components the sand waves may migrate in the opposite of the residual current which is agreement with the observed field data. Residual currents can also influence the fastest growing modes and a larger residual current can even up to total disappearance of the

sand waves. A larger residual current may induce a longer wave length of sand waves. The L_{FGM} is varied with different phases between the different tidal components.

Acknowledgements

The authors would like to acknowledge the support of the National Natural Science Foundation of China (Grant No. 51739010, 51679223, 51709243), the 111 Project (No. B14028), Shandong Provincial Natural Science Key Basic Program (Grant No.: ZR2017ZA0202), a grant of the 7th Generation Ultra-Deep-water Drilling Rig Innovation Project and NWO-ALW, Royal Boskalis Westminster N.V. and Royal Netherlands Institute for Sea Research (NIOZ) for financing the SANDBOX program.

References

Bagnold R A. An approach to the sediment transport problem from general physics[M]. US government printing office, 1966.

Besio G, Blondeaux P, Frisina P. A note on tidally generated sand waves[J]. Journal of Fluid Mechanics, 2003, 485: 171-190.

Besio G, Blondeaux P, Brocchini M, et al. On the modeling of sand wave migration[J]. Journal of Geophysical Research: Oceans, 2004, 109(C4).

Besio G, Blondeaux P, Brocchini M, et al. The morphodynamics of tidal sand waves: A model overview[J]. Coastal engineering, 2008, 55(7-8): 657-670.

Blondeaux P, Vittori G. Flow and sediment transport induced by tide propagation: 1. The flat bottom case[J]. Journal of Geophysical Research: Oceans, 2005, 110(C7).

Blondeaux P, Vittori G. Flow and sediment transport induced by tide propagation: 2. The wavy bottom case[J]. Journal of Geophysical Research: Oceans, 2005, 110(C8).

Blondeaux P, Vittori G. A model to predict the migration of sand waves in shallow tidal seas[J]. Continental Shelf Research, 2016, 112: 31-45.

420 Borsje, B.W., De Vries, M.B., Bouma, T.J., Besio, G., Hulscher, S.J.M.H., Herman P.M.J., 2009a. Modelling
421 biogeomorphological influences for offshore sandwaves. Continental Shelf Research 29, 1289-1301.
422 Borsje, B.W., Hulscher, S.J.M.H., Herman, P.M.J., De Vries, M.B. 2009b. On the parameterization of biological influences on
423 offshore sandwave dynamics. Ocean Dynamics 59, 659-670.
424 Borsje B W, Roos P C, Kranenburg W M, et al. Modeling tidal sand wave formation in a numerical shallow water model: The
425 role of turbulence formulation[J]. Continental shelf research, 2013, 60: 17-27.
426 Borsje B W, Kranenburg W M, Roos P C, et al. The role of suspended load transport in the occurrence of tidal sand waves[J].
427 Journal of Geophysical Research: Earth Surface, 2014, 119(4): 701-716.
428 Burchard H, Craig P D, Gemmrich J R, et al. Observational and numerical modeling methods for quantifying coastal ocean
429 turbulence and mixing[J]. Progress in oceanography, 2008, 76(4): 399-442.
430 Campmans G H P, Roos P C, de Vriend H J, et al. Modeling the influence of storms on sand wave formation: A linear stability
431 approach[J]. Continental shelf research, 2017, 137: 103-116.
432 Campmans G H P, Roos P C, de Vriend H J, et al. The influence of storms on sand wave evolution: a nonlinear idealized
433 modeling approach[J]. Journal of Geophysical Research: Earth Surface, 2018.
434 Damveld J H, Borsje B W, Roos P C, et al. Smart and sustainable design for offshore operations in a sandy seabed-the
435 SANDBOX programme[J]. 2016.
436 Damveld J H, Roos P C, Borsje B W, et al. Modelling the two-way coupling of tidal sand waves and benthic organisms: a linear
437 stability approach[J]. Environmental Fluid Mechanics, 2019: 1-31.
438 de Jong M F, Borsje B W, Baptist M J, et al. Ecosystem-based design rules for marine sand extraction sites[J]. Ecological
439 engineering, 2016, 87: 271-280.
440 Gerwen W V, Borsje B W, Damveld J H, et al. Modelling the effect of suspended load transport and tidal asymmetry on the

441 equilibrium tidal sand wave height[J]. Coastal Engineering, 2018, 136:56-64.

442 Hulscher S J M H, de Swart H E, de Vriend H J. The generation of offshore tidal sand banks and sand waves[J]. Continental Shelf

443 Research, 1993, 13(11): 1183-1204.

444 Hulscher S J M H. Tidal-induced large-scale regular bed form patterns in a three-dimensional shallow water model[J]. Journal of

445 Geophysical Research: Oceans, 1996, 101(C9): 20727-20744.

446 Huntley D A, Huthnance J M, Collins M B, et al. Hydrodynamics and sediment dynamics of North Sea sand waves and sand

447 banks[J]. Phil. Trans. R. Soc. Lond. A, 1993, 343(1669): 461-474.

448 Huthnance J M. On one mechanism forming linear sand banks[J]. Estuarine, Coastal and Shelf Science, 1982, 14(1): 79-99.

449 Komarova N L, Hulscher S J M H. Linear instability mechanisms for sand wave formation[J]. Journal of Fluid Mechanics, 2000,

450 413: 219-246.

451 Lesser G R, Roelvink J A, Van Kester J, et al. Development and validation of a three-dimensional morphological model[J].

452 Coastal engineering, 2004, 51(8-9): 883-915.

453 McCave I N. Sand waves in the North Sea off the coast of Holland[J]. Marine geology, 1971, 10(3): 199-225.

454 Menninga P J. Analysis of variations in characteristics of sand waves observed in the Dutch coastal zone: a field and model

455 study[D]., 2012.

456 Németh A A, Hulscher S J M H, de Vriend H J. Modelling sand wave migration in shallow shelf seas[J]. Continental Shelf

457 Research, 2002, 22(18-19): 2795-2806.

458 Németh A, Hulscher S J M H, de Vriend H J. Offshore sand wave dynamics, engineering problems and future solutions[J].

459 Pipeline and gas journal, 2003, 230(4): 67-69.

460 Németh A A, Hulscher S J M H, Van Damme R M J. Modelling offshore sand wave evolution[J]. Continental Shelf Research,

461 2007, 27(5): 713-728.

462 Rodi W. Turbulence models and their application in hydraulics: a state-of-the-art review, presented by the Int[J]. Assoc. for
463 Hydraulic Research-IAHR-Section of Fundamentals of Division II: Experimental and Mathematical Fluid Dynamics, 1984.
464 Roetert T, Raaijmakers T, Borsje B. Cable route optimization for offshore wind farms in morphodynamic areas[C]//The 27th
465 International Ocean and Polar Engineering Conference. International Society of Offshore and Polar Engineers, 2017.
466 Roos P C, Wemmenhove R, Hulscher S J M H, et al. Modeling the effect of nonuniform sediment on the dynamics of offshore
467 tidal sandbanks[J]. Journal of Geophysical Research: Earth Surface, 2007, 112(F2).
468 Terwindt J H J. Sand waves in the Southern Bight of the North Sea[J]. Marine Geology, 1971, 10(1): 51-67.
469 Tonnon P K, Van Rijn L C, Walstra D J R. The morphodynamic modelling of tidal sand waves on the shoreface[J]. Coastal
470 Engineering, 2007, 54(4): 279-296.
471 van den Berg J. Non-linear sand wave evolution[M]. University of Twente [Host], 2007.
472 Van den Berg J, Sterlini F, Hulscher S J M H, et al. Non-linear process based modelling of offshore sand waves[J]. Continental
473 shelf research, 2012, 37: 26-35.
474 Van Oyen T, Blondeaux P. Tidal sand wave formation: Influence of graded suspended sediment transport[J]. Journal of
475 Geophysical Research: Oceans, 2009, 114(C7).
476 Van Rijn L C. Principles of sediment transport in rivers, estuaries and coastal seas[M]. Amsterdam: Aqua publications, 1993.
477 Van Rijn L C. Unified view of sediment transport by currents and waves. I: Initiation of motion, bed roughness, and bed-load
478 transport[J]. Journal of hydraulic engineering, 2007, 133(6): 649-667.
479 Van Santen R B, De Swart H E, van Dijk T A G P. Sensitivity of tidal sand wavelength to environmental parameters: A combined
480 data analysis and modelling approach[J]. Continental Shelf Research, 2011, 31(9): 966-978.
481 Zang Z P, Cheng L, Gao F P. Application of ROMS for simulating evolution and migration of tidal sand waves[M] // Asian And
482 Pacific Coasts 2011. 2012:1533-1540.

Appendix A. Hydrodynamics model

In the σ coordinate system, the 2DV shallow water equations read,

$$\frac{\partial u}{\partial t}+u\frac{\partial u}{\partial x}+\frac{\omega}{(H+\zeta)}\frac{\partial u}{\partial \sigma}=-\frac{1}{\rho_w}P_u+F_u+\frac{1}{(H+\zeta)^2}\frac{\partial}{\partial \sigma}\left(\nu_T\frac{\partial u}{\partial \sigma}\right) \tag{6}$$

$$\frac{\partial \omega}{\partial \sigma}=-\frac{\partial \zeta}{\partial t}-\frac{\partial\left[(H+\zeta)u\right]}{\partial x} \tag{7}$$

where x denotes the horizontal direction, σ denotes the vertical direction related to σ coordinate system, u is the horizontal velocity and ω is vertical velocity related to σ coordinate system, ρ_w is the water density, H is the water depth below the reference plane, ζ is the free water surface elevation, ν_T is the vertical eddy viscosity which can be evaluated by a specified turbulence closure model, P_u is the hydrostatic pressure gradient, F_u in the momentum equation represents the horizontal Reynold's stress, which is the gradient of shear stress and has the form:

$$F_u=\frac{\partial \tau_u}{\partial x} \tag{8}$$

The shear stress τ_u is,

$$\tau_u=2\nu_H\left(\frac{\partial u}{\partial x}+\frac{\partial u}{\partial \sigma}\frac{\partial \sigma}{\partial x}\right) \tag{9}$$

where ν_H is the horizontal eddy viscosity.

Under the so-called "shallow water assumption", the vertical momentum equation reduces to hydrostatic pressure equation. The hydrostatic pressure gradient can be expressed as:

$$P_u=-\rho_w g\frac{\partial(H+\zeta)}{\partial x} \tag{10}$$

where g is the gravity acceleration.

About the determination of eddy viscosity, most studies on sand waves using stability models adopted a constant or highly simplified relationship, while Borsje et al. (2013) showed that the $k-\varepsilon$ turbulence model could improve the prediction of wavelength and migration rate of sand waves considerably. Turbulent kinetic energy k and energy dissipation ε can be solved by transport equations. For details on turbulence model and $k-\varepsilon$ equations see Rodi (1984) and Burchard et al. (2008).

At the surface, a no-stress condition is applied and vertical velocity ω is set to zero:

$$\rho_w \frac{\nu_T}{(H+\zeta)} \frac{\partial u}{\partial \sigma}\bigg|_{\sigma=0} = 0, \quad \omega|_{\sigma=0} = 0 \tag{11}$$

At the sea bed which is the closed boundary, the tangential shear stress is calculated based on a logarithmic law of the wall:

$$\tau_b \equiv \rho_w \frac{\nu_T}{(H+\zeta)} \frac{\partial u}{\partial \sigma}\bigg|_{\sigma=-1} = \rho_w u_* |u_*|, \quad \omega|_{\sigma=-1} = 0 \tag{12}$$

where τ_b is the bed shear stress, u_* is the friction velocity which is determined by the logarithmic-law related to the velocity gradient at the lowest grid point.

Under the assumption of a logarithmic velocity profile, the relationship between depth-averaged velocity and friction velocity is as follows:

$$u_r = \frac{u_*}{\kappa} \ln\left(1 + \frac{H+\zeta}{e z_0}\right) \tag{13}$$

where κ is the Kármán's constant, z_0 is the bed roughness height, which reads:

$$z_0 = \frac{H+\zeta}{e^{1+\frac{\kappa C_D}{\sqrt{g}}} - e} \tag{14}$$

where C_D is Chézy coefficient.

Appendix B. Sediment transport and morphological evolution model

Sediment can be transported as bedload and suspended load. The coordinate system used to determine the sediment transport is based on Cartesian z coordinate system.

The vertical velocity ω solved in hydrodynamics model is related to the moving σ plane (Lesser et al., 2004). The vertical velocity w in the z coordinate system can be expressed in the horizonal velocities, water depths, water levels, and vertical coordinate velocity according to:

$$w = \omega + u\left(\sigma\frac{\partial(H+\zeta)}{\partial x}+\frac{\partial\zeta}{\partial x}\right)+\left(\sigma\frac{\partial(H+\zeta)}{\partial t}+\frac{\partial\zeta}{\partial t}\right) \tag{15}$$

Suspended sediment transport is modeled by the 2DV advection-diffusion equation, which reads:

$$\frac{\partial c}{\partial t}+\frac{\partial(cu)}{\partial x}+\frac{\partial(w-w_s)c}{\partial z}=\frac{\partial}{\partial x}\left(\varepsilon_{s,x}\frac{\partial c}{\partial x}\right)+\frac{\partial}{\partial z}\left(\varepsilon_{s,z}\frac{\partial c}{\partial z}\right) \tag{16}$$

where c is the suspended sediment concentration, w is the vertical velocity related to z coordinate system, w_s is the sediment settling velocity, $\varepsilon_{s,x}$ and $\varepsilon_{s,y}$ are horizontal and vertical eddy diffusivities, respectively, which are assumed to be equal to the horizontal and vertical eddy viscosity.

$$w_s=\frac{10\nu}{d_{50}}\left(\sqrt{1+\frac{0.01(\rho_s/\rho_w-1)gd_{50}}{\nu^2}}-1\right) \tag{17}$$

where ν is the water viscosity coefficient, ρ_s is sediment density.

According to Van Rijn (2007), sediment transport above the reference height ($a=0.01H$) is regarded as suspended load, which can be calculated as:

$$S_s=\int_a^{(H+\zeta)}uc\ \mathrm{d}z \tag{18}$$

where S_s is suspended load transport.

The bedload can be calculated using the approximation method proposed by Van Rijn (1993), which reads:

$$S_b'=0.5\rho_s d_{50}u_*'d_*^{-0.3}T \tag{19}$$

where S_b' is the bedload transport without considering slope effect, u_*' is the effective bed-shear velocity, d_* is non-dimensional particle diameter and T is non-dimensional bed-shear stress.

$$u_*' = u_* \mu_c^{0.5} \tag{20}$$

where μ_c is efficiency factor current,

$$\mu_c = \frac{f_c'}{f_c} \tag{21}$$

where f_c' and f_c are grain-related and total current-related friction factors, respectively.

$$f_c' = 0.24\left[\log_{10}\left(\frac{12(\mathrm{H}+\zeta)}{3d_{90}}\right)\right]^{-2} \tag{22}$$

$$f_c = 0.24\left[\log_{10}\left(\frac{12(\mathrm{H}+\zeta)}{k_s}\right)\right]^{-2} \tag{23}$$

where d_{90} is 90% sediment passing size, $d_{90} = 1.5d_{50}$, k_s is the Nikuradse roughness length, $k_s = 30z_0$.

$$d_* = d_{50}\left[\frac{(\rho_s/\rho_w - 1)g}{\nu^2}\right]^{1/3} \tag{24}$$

$$T = \frac{\mu_c \tau_b - \tau_{cr}}{\tau_{cr}} \tag{25}$$

where τ_{cr} is critical bed shear stress, which reads,

$$\tau_{cr} = (\rho_s - \rho_w) g d_{50} \theta_{cr} \tag{26}$$

where θ_{cr} is the threshold parameter calculated according to van Rijn (1993) as a function of the non-dimensional grain size.

Bedload transport should be adjusted by bed slope effect as it is affected by bed level gradients. The adjusted bedload transport is defined as:

$$S_b = \alpha_s S_b' \tag{27}$$

where S_b is the adjusted bedload transport and α_s is a correction parameter for slope effect, which can be calculated with Bagnold (1966):

$$\alpha_s = 1 + \alpha_{bs}\left(\frac{\tan(\phi)}{\cos\left(\tan^{-1}\left(\frac{\partial z}{\partial s}\right)\right)\left(\tan(\phi) - \frac{\partial z}{\partial s}\right)} - 1\right) \tag{28}$$

where ϕ is the repose angle of sediment, $\partial z / \partial s$ is the bed slope in the direction along to the unadjusted bedload transport vector, α_{bs} is a user-defined tuning parameter.

The bed level change can be evaluated by sediment continuity equation (Exner equation):

$$(1 - p_{or})\frac{\partial z_b}{\partial t} + \frac{\partial}{\partial x}(S_b + S_s) = 0 \tag{29}$$

in which $p_{or} = 0.4$ is the bed porosity.

Modeling the formation and migration of sand waves: The role of tidal forcing, sediment size and bed slope effects

Zhenlu Wang[1], Bingchen Liang[1,2,*], Guoxiang Wu[1,2], Borsje B. W.[3]

Highlights:

(1). After calibration of the slope parameter for a specific location, the sand wave length is reproduced good compared to field observations

(2). The migration rate is considerably better predicted with the Delft3D model compared to the Blondeaux model. This is because of the more accurate turbulence formulation (k- ε) in the Delft3D model, while the constant eddy viscosity overestimates the transport rates and thereby the migration rates.

(3). Residual currents and higher harmonics not only influence the migration rates but also the fastest growing modes (even up to total disappearance of the sand waves)

Dear Editor,

I am submitting our manuscript entitled "**Modeling the formation and migration of sand waves: The role of tidal forcing, sediment size and bed slope effects**" by Zhenlu Wang, Bingchen Liang, Guoxiang Wu and Borsje B. W. to *Continental Shelf Research* as a full-length article. We would be grateful if the manuscript could be reviewed and considered for publication in *Continental Shelf Research*.

This manuscript has not been published or presented elsewhere in part or in entirety and is not under consideration by another journal. All the authors have approved the manuscript and agree with submission to your esteemed journal. There are no conflicts of interest to declare.

Thank you and best regards!

Sincerely,

Bingchen Liang

College of Engineering

Ocean University of China

Qingdao 266100

China

Email: bingchen@ouc.edu.cn

Tel: 86-532-66783719

Fax: 86-532-66781550